

Article

Experimental Study of the Dynamic Short-Circuit Withstand Capability of an 8400 kVA Power Transformer Specially Designed for Photovoltaic Applications

Cristian-Eugeniu Sălceanu, Cătălin Dobrea, Daniel Ocoleanu, Marcel Nicola , Daniela Iovan * and Maria-Cristina Nițu *

Research and Development Department, National Institute for Research, Development and Testing in Electrical Engineering—ICMET Craiova, 200746 Craiova, Romania; csalceanu@icmet.ro (C.-E.S.)

* Correspondence: pdaniela@icmet.ro (D.I.); cristinaniu@icmet.ro (M.-C.N.)

Abstract: This article, besides offering data of great value for any designer of high-power short-circuits of special three-winding design, illustrates the correlation with the corresponding FRA measurements, validating this type of measurement. The frequency response measurements can provide data about the transformer's status after it is put into service, its vulnerability in incipient states, and, particularly for this type of transformer, its insulation, which is the subject of high dielectric stress due to its inverter working regime. This article presents the behavior of a three-phase 8400 kVA medium-voltage step-up transformer (corrugated hermetic tank) specially designed for photovoltaic applications during short-circuit tests. This transformer, fed by two inverters, has two secondaries with elliptical windings (non-circular aluminum foil for LV windings and an aluminum conductor for HV windings). Various experiments were performed, including measurements of winding resistance, measurements of voltage ratio, measurements of short-circuit impedance and load loss on three tappings, measurements of no-load loss and current, a frequency response analysis, and short-circuiting. These experiments were performed to study the behavior of the transformer, which, in real life, is powered by photovoltaic inverters on the LV side that feed into the MV grid on the HV side, making it the interface between the photovoltaic inverter and the MV grid. An auxiliary supply transformer may be connected to the LV side. Given these elements, concerning both the importance and the particularities of the problem studied, we can say that this article represents a niche study on the guarantee of good functioning and safety in operation given the passing of the test to withstand the dynamic effects of short-circuiting.

Keywords: distribution transformer; renewable energy; photovoltaic generation; short-circuit; frequency response; windings



Citation: Sălceanu, C.-E.; Dobrea, C.; Ocoleanu, D.; Nicola, M.; Iovan, D.; Nițu, M.-C. Experimental Study of the Dynamic Short-Circuit Withstand Capability of an 8400 kVA Power Transformer Specially Designed for Photovoltaic Applications. *Machines* **2023**, *11*, 969. <https://doi.org/10.3390/machines11100969>

Academic Editor: Ahmed Abu-Siada

Received: 25 August 2023

Revised: 13 October 2023

Accepted: 14 October 2023

Published: 17 October 2023



Copyright: © 2023 by the authors. Licensee MDPI, Basel, Switzerland. This article is an open access article distributed under the terms and conditions of the Creative Commons Attribution (CC BY) license (<https://creativecommons.org/licenses/by/4.0/>).

1. Introduction

Socio-economic and environmental requirements for power generation have increased the number of distributed photovoltaic (DPV) installations worldwide. In the DPV system, electricity is generated by converting solar energy into a direct current (DC) using photovoltaic (PV) cells, usually made of silicon. The direct current generated is then converted to a three-phase alternating current (AC) by inverters and connected to the grid via a step-up transformer [1–3].

Currently, there are limitations on the power rating and voltage level of the inverter. Accordingly, one, two, or three inverters are connected to the LV winding of step-up transformers designed according to current standards [4–7].

The transformers commonly used for the DPV system are as follows: a two-winding transformer fed by one inverter; a three-winding transformer fed by two inverters (this transformer will have two secondary windings); and a four-winding transformer fed by three inverters (this transformer will have three secondary windings).

Demand for DPV equipment is growing due to the benefits of carbon-free power, lower costs, and related benefits [8,9].

The paper [10] presents the special technical characteristics of the transformer for DPV applications, design considerations, and various design options. In addition, the design parameters and test results of a transformer that was manufactured for DPV applications are presented.

The power transformer is a key piece of equipment in power grids, and its reliability directly affects the reliability of the power system. Defective transformer cores or windings can increase losses and cause the transformer to overheat, affecting its stable operation. The no-load losses of the transformer reflect the condition of the iron core and windings. They are typically measured using offline no-load tests, which are difficult to implement in the field [11–14].

Natural esters are of growing interest worldwide, with liquid-insulated transformer designers increasingly preferring this technology. Users are still conservative as the voltage level increases, although there is a clear need to apply the same technology to the power transformer. The paper [15] presents the possibility of using natural ester fluid in power transformers by performing a comparative test on a real 220 kV/16 MVA power transformer designed for mineral oil. All routine and type tests were carried out on the actual 220 kV/16 MVA power transformer and then a natural ester insulating fluid (FR3) was used.

The economic and industrial environment is totally dependent on electricity, and the quality of the power grid is of paramount importance. As industrial loads increase, major power outages have occurred, prompting energy companies to seek viable solutions to ensure the stability of their grids. There are many reasons for power outages, from problems to physical force or natural disasters. In economic terms, the cost of such a disruption to the energy industry and society can be enormous. The paper [16] examines three areas of action that are key to addressing resilience: prevention, protection, and response. The paper also presents a new solution for rapid response when a quick replacement is required.

Several papers present simulations for the residential smart grid based on the semiconductor transformer, and in [17], a special case is presented that allows the study of any operating situation during power supply by the optimal configuration of the circuits. The result is an intelligent network of converters matched to the required power levels.

The literature examines situations where power plants need to be restarted in the event of a total or partial blackout without involving the external power transmission system. Restart solutions based on energy storage are presented, as renewable electricity generation is limited by weather conditions [18]. Grid-scale energy storage can provide reliable bus voltage to access PV generation. The solar storage system can then ensure the smooth start-up of ancillary equipment for the traditional power plant to restore power for critical operations.

The treatment of PV production series over time often faces the challenge of unifying series granularity when generating a predictive model. This may limit the generation of a dataset in terms of the time period covered and the number of examples. In addition, models built with static granularity data tend to exhibit rigidity when faced with variations in granularity, invalidating them for scenarios different from the data on which they were trained. To address this problem, a new method that does not vary in granularity, called Synthesis, is presented in [19].

To significantly improve differential protection performance, algorithms have been developed that reduce the current transformer requirements and also provide improvements in the case of faults caused by CT saturation [20]. In another paper [21], an approach has been developed that uses the path of differentiated transformer currents to make a clear distinction between inrush currents and an internal fault. Simulations of various transformer differential protection schemes have been performed using MATLAB and have been found to be effective and reliable in solving problems associated with differential

relays, such as changing hubs, inherent phase changes in currents in the transformer, and transformer ratios.

As power systems have adapted to irregular operation, power transformers have shown limited ability to support the new functionalities introduced by operational disturbances [22–25]. Such functionalities include power flow control, the integration of distributed generation and storage, voltage and frequency regulation, power quality improvement, and DC load integration [24–35].

The high concentration of single-phase PV installations on low-voltage distribution feeders contributes significantly to voltage spikes and unbalance [1–4]. This often results in limited energy production from PV systems (due to automatic inverter shutdown) and failures of other power-consuming equipment.

The paper [26] discusses the principle of operation of a differential transformer and an automatic series voltage regulator and presents the results of simulations and measurements on the effectiveness of increasing the voltage and attenuating the unbalance using these devices in two low-voltage networks located within the Virtual Green energy cluster.

Paper [27] presents the results of applying more accurate sizing to step-up transformers based on the actual load profile when used for solar, thermal, or photovoltaic generation.

As solar power generation can have peaks and troughs throughout the day, it is advisable to set the transformer to a certain value to prevent it from aging, so that the transformer is not oversized and can provide the same reliable and robust service for a sufficient number of years compared to today's traditional approach.

This paper presents an experimental study of the behavior at dynamic short-circuit withstand of a special-design power transformer used in distributed photovoltaic systems. After the high-power short-circuit tests, an FRA analysis is carried out to prove that it is sufficient to show that the transformers need more careful analysis or even maintenance. Because the transformer is used in DPV installations, it is subject to many unusual electrical operating conditions and cannot always be subjected to a detailed inspection, so the purpose of this article is to show that the FRA can detect minor faults caused by short circuits.

This type of fault can occur because:

- The transformer is connected to the photovoltaic directly or through switchgear and it can often be subject to load rejection conditions and special load rejection conditions;
- The waveform can be severely distorted;
- The transformer may be subjected to frequent overcurrents;
- Asymmetrical voltages from an essentially sinusoidal wave;
- Abnormal harmonic currents, which can cause excessive losses and abnormal heating, are involved in DPV installations.

The most valuable feature of the FRA is that it can be carried out on-site and we suggest that is often required for this particular type of transformer.

After the short-circuit test and routine analysis, a frequency response analysis is carried out to prove that it can detect changes in the active part (windings, leads, and core). The oscillogram shows even the smallest damage after a through fault.

It is preferable to carry out the measurement at the factory or on-site when commissioning the transformer and use the data as a reference. On completion of the standard measurements, the measurement leads and earth connections should be disconnected and then the first measurement repeated and recorded. This check is necessary to evaluate the repeatability and usable diagnostic frequency range under the specific conditions of the measurement.

In addition to the data, which are of great value to any designer of high-power transformers with a special three-winding design, this article shows the correlation with the corresponding FRA measurements, validating this type of measurement. It is also important that frequency response measurements are always made in a consistent manner and that all details are systematically recorded. It is important to emphasize that all data relevant to each frequency response measurement is recorded in detail so that any discrepancies can be understood.

Starting from this general image of the operation of a PV-based power generation assembly and its injection into the grid, this paper presents a niche element in the study of ensuring the proper functioning and operational safety given the passing of the test to withstand the dynamic effects of short-circuiting.

Thus, there is very little structured information in the literature on the performance in such a test of one of the most important elements in the chain of elements presented above on PV-based energy production and supply to the main power network.

The main contributions of this article are the synthetic presentation of the phenomenology of the short-circuit and FRA tests, the results of the routine experiments, and the analysis of the behavior at short-circuit and FRA experiments.

We prove that FRA analysis is enough to show that the transformers need a more careful analysis or even maintenance. It shows the FRA can detect minor to major faults caused by short-circuits. It is proven that after the short-circuit, the frequency response analysis is made to prove that it can detect changes to the active parts.

The rest of the article is structured as follows. In Section 2, the design features of transformers used in distributed photovoltaic generation are presented, while experiments of an 8.4 MVA, 33 kV/0.66 – 0.66 kV transformer are presented in Section 3. In Section 4, conclusions and ideas for future work are presented.

2. Design Characteristics of Transformers Used in Distributed Photovoltaic Systems

Power transformers are one of the most important pieces of equipment in an electrical network. Dry or oil-immersed transformers have evolved a lot recently with the advent of new materials and technologies.

The recent energy crisis and the race to find new forms of green energy that can be converted into electricity have also led distribution transformers to adapt to harmonics generated by electrical inverters and asymmetries due to unbalanced consumers or other causes.

With low losses, voltage ratios adapted to requirements, operating as step-up or step-down transformers depending on the time of day, and with powers up to 10 MVA, transformers must meet all individual, type, or special requirements imposed by specific standards. It should be noted that the presence of harmonics causes additional losses in the transformer (in the windings and the magnetic core), additional heating, and, therefore, a poor thermal class of transformers in the substations.

The ever-increasing amount of energy generated by photovoltaic systems and converted into electricity, transformed and distributed in medium-voltage networks, has created new challenges for transformer designers in finding solutions for specific operating regimes in inverter circuits.

The direct current generated by the photovoltaic cells is converted into an alternating current by means of one or more inverters connected to the low-voltage windings of a step-up transformer. Figure 1 shows the general layout of a system.

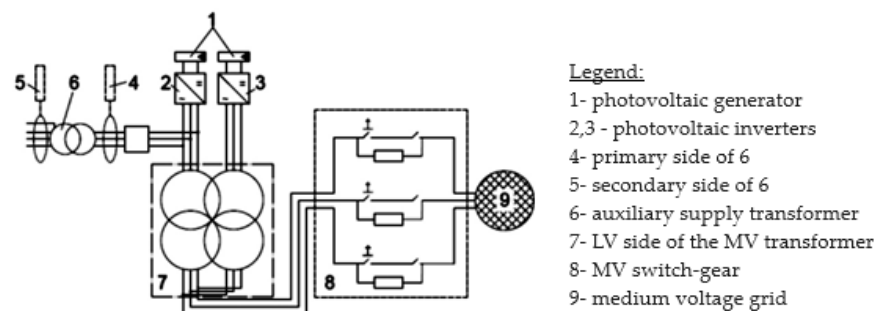


Figure 1. Schematic layout of the MV system, including the inverter and MV switchgear.

In Figure 1, the power from a photovoltaic generator (1) will be provided by photovoltaic inverters (2, 3) on the LV side of the MV transformer (7), which feeds into the

medium voltage grid (9) on the HV side of the MV transformer with a regular MV switch-gear (8). The MV transformer is the interface between the photovoltaic inverter and the MV grid. On the LV side, an auxiliary supply transformer (6) is connected on the primary side (4) to the transformer protection device, and the secondary side of (6) is (5).

The technical solutions used to build these transformers depend on the manufacturer, but the general idea is to use the type with two concentric secondary windings with half windings for HV and LV. As current imbalances, high losses, and transformer heating occur when an inverter is idle, the solution is to use half windings on LV and HV, distributed as shown in Figure 2.

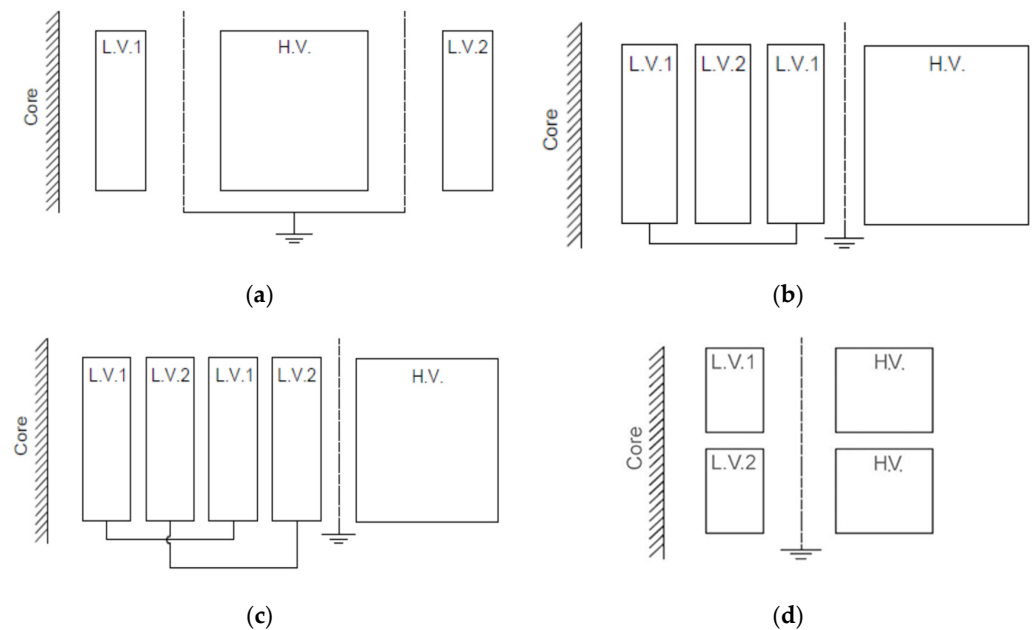


Figure 2. Various winding configurations: (a) concentric winding; (b) concentric winding with vertically interleaved LV winding (Type-A); (c) concentric winding with vertically interleaved LV winding (Type-B); (d) vertically stacked LV winding.

Figure 2 shows the most common types of transformers used in the distribution of energy produced by photovoltaic panels, with three types of windings and two secondary windings. The impedance in the low-voltage to high-voltage winding must be equal, so it is necessary to set up LV1-HV-LV2 windings. In Figure 2a, it is difficult to match the impedance of the LV1-LV2 and LV2-HV windings because one is very close to the core and the other very far away, resulting in very different short-circuit impedance values and therefore short-circuit currents across the two windings. In Figure 2b, the LV1-HV and LV2-HV impedance values are approximately equal, but the LV1-LV2 impedance is relatively low, resulting in high short-circuit currents. In Figure 2c, the LV1-HV and LV2-HV impedance values are approximately the same, but the LV1-LV2 impedance is relatively low and the manufacturing cost is much higher than in (b). Split concentric LV windings have the same impedance as HV windings, but are very difficult to achieve, requiring many LV connections and high-current circuits in the case of short-circuiting and implicitly uncontrollable electrodynamic forces. In Figure 2d, the magnetic impedance values LV1-HV and LV2-HV are almost equal, the LV winding is split axially, but this type of construction is large and LV connections are difficult to achieve. Therefore, design (d) is preferred by most manufacturers.

The technical solutions shown in Figure 2 with distributed half windings on LV and HV are adopted because when an inverter is inactive, unbalanced currents, high losses, and transformer heating occur.

The following situations may occur during transformer operation:

- Unbalanced voltages, which can create an unbalanced current system with known consequences;
- Unbalance in the windings and high iron flux when connecting an inverter;
- Increased magnetizing current and inrush current due to a DC in the windings;
- Unsynchronized waveforms at the inverter output, leading to a change in the waveform and the appearance of harmonics that disturb the magnetic flux of the transformer;
- Fast-rising waveform due to inverter switching, which produces voltage pulses with a large du/dt slope in the low voltage winding, which must withstand these dielectric stresses. For this purpose, grounded shields are used between the HV and LV windings;
- Some of the transformers in generation systems operate all day, 10–12 h/day, but when the system stores energy in battery systems, the transformer operates continuously under load.

Other systems keep the transformer energized even when no power is being generated, causing no-load losses, so the transformer is designed with low no-load losses. However, if the system involves repeated connections and disconnections, the transformer must withstand the effects of this regime.

Considering that transformers supplied by inverters are fed by low voltage windings with high harmonic content but also with frequent transients, their specific characteristics are as follows:

- The most common type of transformer is the three-winding type, two LV and one HV;
- The arrangement of the windings in relation to the magnetic core must take into account the asymmetrical and unbalanced regimes by splitting, interleaving, and shielding them, as shown in Figure 2;
- The short-circuit impedance values of the two LV windings must be equal, although this is difficult to achieve;
- The insulation of the LV windings must be designed to withstand switching surges with a rise rate of up to $(0.300\text{--}0.400)$ kV/ μ s. Typically, any switching surge in the LV windings caused by inverters propagates to the HV winding with the voltage ratio, and to prevent this phenomenon, the LV winding is electrostatically shielded;
- The transformer must be designed with low no-load losses, as it may have long idle periods;
- The cooling system must be adapted to the location and whether the transformer is operating in a substation or outdoors;
- If the transformer operates in a substation, the thermal class (5, 10, 15, or 20) representing the percentage of the transformer under load must be determined [28];
- It is necessary to take into account the transformer load curve, the effect of harmonics, and the effect of reactive load;
- Short-circuit calculations must take into account the layout of the windings (short-circuit impedance) and the additional connections on the LV winding;
- The ability of the transformer to withstand the short-circuit is verified by special tests where the short-circuit conditions are determined by the manufacturer, but usually, [28] is considered;
- It is known that when a transformer is connected in an open circuit, a peak current occurs, called an inrush current, which is the peak value of the transient no-load current and can be several hundred times higher than the value of the stabilized no-load current;
- Considering the goal of “green energy”, the environmental impact of mineral oil used in oil transformers and the choice of a dry-type transformer must be taken into account.

The scope of this paper is to analyze the short-circuit behavior of solar DPV transformers because it is an area under continuous development with various construction possibilities, and any developer can take the knowledge for future development.

3. Experiments on an 8.4 MVA Transformer; 33 kV/0.66 – 0.66 kV

This section presents experiments comprising individual types and special tests required by [1–9], ref. [28], carried out on an 8.4 MVA transformer to verify its short-circuit behavior.

3.1. Technical Characteristics

The 8.4 MVA transformer with one 33 kV HV winding and two 0.66 kV LV windings had the following characteristics: transformer rated power, $S_N = 8400$ kVA; HV side voltage, $U_{HV} = 33 \text{ kV} \pm 2 \times 2.5\%$; LV side voltage, $U_{LV} = 0.66 \text{ kV} - 0.66 \text{ kV}$; rated current of energized winding, $I_N = 147 \text{ A}/3674 - 3674 \text{ A}$; vector group, $\Delta Y11Y11$; cooling type, Oil Natural Air Natural (ONAN); windings, aluminum conductor, non-circular (oval).

Short-circuit voltages:

$$U_{k75^\circ} = 7.35\% \text{-LV } 2u\text{-}2v\text{-}2w;$$

$$U_{k75^\circ} = 7.49\% \text{-LV } 3u\text{-}3v\text{-}3w.$$

Rated current short-circuit losses:

$$P_{k75^\circ} = 28,270 \text{ W-}2u\text{-}2v\text{-}2w;$$

$$P_k = 30,506 \text{ W-}3u\text{-}3v\text{-}3w.$$

No-load losses according to rated conditions $P_0 = 6200 \text{ W}$:

1U-1V-1W-HV winding;

2u-2v-2w-LV winding no. 1;

3u-3v-3w-LV winding no. 2.

3.2. Design Features

The transformer was designed with concentric windings, divided by parallel HV and separate LV half windings, in mineral oil in a sealed tank, and the oval shape of the aluminum core and coils in the column section. The LV windings were made of aluminum foil and the HV windings were made of profiled aluminum conductors with paper insulation.

The wiring diagram and the vector group is $\Delta Y11Y11$ and, normally, to avoid unbalances caused by single-phase consumers, the neutral is not accessible.

LV winding has additional insulation to reduce surges during inverter-generated switching.

No-load losses are reduced compared to a typical distribution transformer. The appearance of the transformer (active part) is shown in Figure 3.

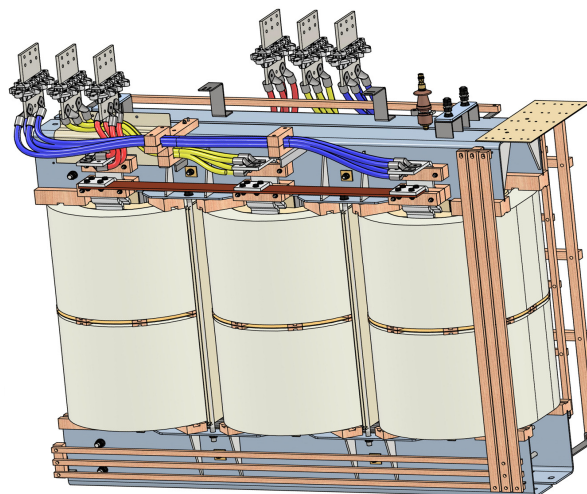


Figure 3. Three-dimensional representation of the MV transformer used for the tests.

3.3. Experimental Technical Conditions

In general, the assessment of a product for validation purposes is carried out against internal or international standards that take into account the normal or special functional requirements specific to the installation site.

The tests carried out to evaluate the 8.4 MVA transformer closely follow the tests required by [1–9], ref. [28] and include individual types and special tests.

Individual (routine) tests:

- Measurement of the ohmic resistance of the windings;
- Measurement of the transformation ratio and vector group determination;
- Measurement of losses and short-circuit impedance;
- Measurement of losses and no-load current;
- Dielectric tests with:
 - Applied voltage;
 - Induced voltage;
 - Tap-changer testing.

Type tests:

- Temperature rise tests;
- Dielectric tests including lightning impulse tests;
- Noise level determination;
- Short-circuit tests.

All the tests mentioned are important, but the purpose of the tests is to verify the short-circuit behavior of the transformer, and this verification requires individual tests before and after the short-circuit for validation.

In addition, after the short-circuit, the tank is removed from the transformer and the active part is carefully inspected.

The frequency response method (FRA) is also recommended to assess the condition of the transformer under short-circuit conditions.

The frequency response method (FRA) consists of measuring the amplitude ratio and the phase difference on the windings when a frequency signal in a specified range (10–106 Hz) is injected and comparing them (before and after short-circuit).

3.4. Results of Routine Tests

Measurements of winding resistance values, voltage ratio, wiring diagram and vector group, no-load, and short-circuit losses in the initial state before the short-circuit tests are shown in Table 1 and repeated after the short-circuit for comparison.

In the short-circuit tests, the 8400 kVA transformer with two identical LV windings was treated as two transformers with a common 2×4200 kVA HV winding, and measurements were taken separately on each LV winding with a common HV winding.

Table 1. Values obtained from the measurements of winding resistance values, voltage ratio, wiring diagram and vector group, no-load, and short-circuit losses in the initial state.

Measurement of Winding Resistance Temperature 20.4 (°C)	Tape	1U1V (mΩ)	1V1W (mΩ)	1U1W (mΩ)
HV winding	1	427.96	426.57	425.89
	2	415.99	415.97	415.27
	3	405.42	405.34	404.76
	4	395.13	395.00	394.41
	5	384.68	384.82	384.10

Table 1. Cont.

Measurement of Winding Resistance Temperature 20.4 (°C)	Tape	1U1V (mΩ)			1V1W (mΩ)			1U1W (mΩ)				
LV winding		2U2V (μΩ)			2V2W (μΩ)			2W2U (μΩ)				
		403.48			429.86			430.57				
		3U3V(μΩ)			3V3W(μΩ)			3W3U(μΩ)				
		440.89			440.53			454.46				
Measurement of voltage ratio vector group Dyn11	1U1W/2V2W (Jumper 1W-1V)				1V1U/2W2U (Jumper 1U-1W)				1W1V/2U2V (Jumper 1V-1U)			
	Tape	Calc.	Meas.	Dev.	Tape	Calc.	Meas.	Dev.	Tape	Calc.	Meas.	Dev.
	1	90.933	90.811	−0.13	1	90.933	90.811	−0.13	1	90.933	90.810	−0.13
	2	88.768	88.675	−0.10	2	88.768	88.676	−0.10	2	88.768	88.713	−0.06
	3	86.603	86.558	−0.05	3	86.603	86.573	−0.03	3	86.603	86.597	−0.01
	4	84.437	84.456	0.02	4	84.437	84.470	0.02	4	84.437	84.469	0.04
	5	82.272	82.340	0.08	5	82.272	82.340	0.08	5	82.272	82.361	0.11
	1U1W/3V3W (Jumper 1W-1V)				1V1U/3W3U (Jumper 1U-1W)				1W1V/3U3V (Jumper 1V-1U)			
	Tape	Calc.	Meas.	Dev.	Tape	Calc.	Meas.	Dev.	Tape	Calc.	Meas.	Dev.
	1	90.933	90.812	−0.13	1	90.933	90.829	−0.11	1	90.933	90.813	−0.13
	2	88.768	88.712	−0.06	2	88.768	88.714	−0.06	2	88.768	88.713	−0.06
	3	86.603	86.597	−0.01	3	86.603	86.597	−0.01	3	86.603	86.597	−0.01
	4	84.437	84.470	0.04	4	84.437	84.470	0.04	4	84.437	84.488	0.06
	5	82.272	82.352	0.10	5	82.272	82.366	0.11	5	82.272	82.376	0.13
	Measurement of short-circuit impedance and load lose TAP POSITION-1	4200 kVA 2U-2V-2W short-circuited				4200 KVA 3U-3V-3W short-circuited						
		Current A	Voltage V	Power W		Current A	Voltage V	Power W				
U		69.420	1419	8576	U	69.582	1454	8845				
V		70.282	1409	8979	V	70.404	1443	10,344				
W		69.677	1414	10,480	W	69.198	1450	11,222				
Avrg.		69.793	1414	Σ: 28,035	Avrg.	69.728	1449	Σ: 30,411				
Δcorr.		1.0027	Γcorr.	1.0054	Δcorr.	1.0036	Γcorr.	1.0072				
		I _n : 69.982 A	U _n : 2449.12 V	P _k : 28,187 W		I _n : 69.982	U _n : 2509.74 V	P _k : 30,633 W				
		P _{k(75 °C)} = 27,776 W	U _{k(75 °C)} % = 7.11			P _{k(75 °C)} = 29,973 W	U _{k(75 °C)} % = 7.30					
Measurement of short-circuit impedance and load lose TAP POSITION-3		4200 kVA 2U-2V-2W short-circuited				4200 KVA 3U-3V-3W short-circuited						
		Current A	Voltage V	Power W		Current A	Voltage V	Power W				
	U	73.060	1335	8597	U	73.273	1369	8885				
	V	73.957	1325	9013	V	74.142	1359	10,432				
	W	73.304	1330	10,531	W	72.820	1365	11,285				
	Avrg.	73.440	1330	Σ: 28,141	Avrg.	73.412	1364	Σ: 30,662				
	Δcorr.	1.0005	Γcorr.	1.0011	Δcorr.	1.0009	Γcorr.	1.0018				
		I _n : 73.481 A	U _n : 2303.63 V	P _k : 28,172 W		I _n : 73.481 A	U _n : 2363.09 V	P _k : 30,660 W				
		P _{k(75 °C)} = 27,823 W	U _{k(75 °C)} % = 7.01			P _{k(75 °C)} = 30,054 W	U _{k(75 °C)} % = 7.20					
	Measurement of short-circuit impedance and load lose TAP POSITION-5	4200 kVA 2U-2V-2W short-circuited				4200 KVA 3U-3V-3W short-circuited						
		Current A	Voltage V	Power W		Current A	Voltage V	Power W				
U		77.073	1256	8682	U	77.425	1291	8979				
V		77.966	1246	9083	V	78.281	1280	10,548				
W		77.308	1251	10,629	W	76.899	1286	11,407				
Avrg.		77.449	1251	Σ: 28,394	Avrg.	77.535	1286	Σ: 30,934				
Δcorr.		0.9987	Γcorr.	0.9974	Δcorr.	0.9975	Γcorr.	0.9951				
		I _n : 77.348 A	U _n : 2166.80 V	P _k : 28,320 W		I _n : 77.348 A	U _n : 2226.84 V	P _k : 30,785 W				
		P _{k(75 °C)} = 28,012 W	U _{k(75 °C)} % = 6.93			P _{k(75 °C)} = 30,225 W	U _{k(75 °C)} % = 7.12					

Table 1. Cont.

Measurement of Winding Resistance Temperature 20.4 (°C)	Tape	1U1V (mΩ)			1V1W (mΩ)			1U1W (mΩ)				
		Excitation Factor 90%			Excitation Factor 100%			Excitation Factor 110%				
Measurement of no-load loss and current		Current A	Voltage V	Power W	Current A	Voltage V	Power W	Current A	Voltage V	Power W		
	U	6.212	344.54	2025.0	U	10.646	382.74	3031.0	U	51.161	417.16	8525.0
	V	3.654	342.34	1070.0	V	7.034	379.6	1328.0	V	36.670	421.66	725.2
	W	5.926	342.03	1558.0	W	11.065	380.88	1842.0	W	55.754	418.76	385.8
	Avrg.	5.264	342.97	Σ: 4653	Avrg.	9.582	381.07	Σ: 6201	Avrg.	47.862	419.20	Σ: 9636
	$V_{RMS} = 594.6$ V		$V_{MEAN} = 594.0$ V		$V_{RMS} = 661.7$ V		$V_{MEAN} = 660.0$ V	P_0 GUARANTEED = 7200 W + 15%		$V_{RMS} = 739.9$ V		$V_{MEAN} = 726.1$ V
	$I_0 = 5.264$ A		$I_0 = 0.14\%$ $P_0 = 4649$ W		$I_0 = 9.582$ A		$I_0 = 0.26\%$ $P_0 = 6185$ W		$I_0 = 47.862$ A		$I_0 = 1.30\%$ $P_0 = 9453$ W	

Calc.—calculated; Meas.—measured; Dev.—deviation; Avrg.—average; Δcorr.—current correction; Γcorr.—power correction; Σ—sum power.

The wiring diagrams, vector groups, and transformation ratios do not deviate from the designed (calculated) values by more than 0.14%.

As far as short-circuit losses and short-circuit impedance (voltage) are concerned, no matter how much it was intended, identical windings and connections could not be achieved due to the cumbersome technology, so there is a significant difference between the short-circuit voltages.

Losses in 2u2v2w LV windings were approximately 28,000 W, and in 3u3v3w, they were approximately 30,000 W. This is also observed when measuring the ohmic resistance of the LV windings, which is about 5% higher on 3u3v3w windings further away from the core (above 3u3v3w).

The short-circuit voltage of the 3u3v3w LV winding is also approximately 3% higher than that of the 2u2v2w LV winding.

At no load, the following values were obtained, $I_0 = 9.58$ A, $P_0 = 6185$ w, and $I_0 = 0.26\%$, which are quite low compared to similar transformers but used for a different purpose.

Dielectric tests with applied voltage, induced voltage, and impulse voltage are also criteria for evaluating short-circuit behavior. They are performed before and after the short-circuit test but are not included in this paper. Apart from the visual inspection during the removal of the active part, the most important tests for the short-circuit behavior of the transformer are the measurements of the short-circuit reactance values. Measured before and after the test with high-precision electronic bridges (0.2% class), they reveal the slightest misalignment or deformation of the coils, terminals, and magnetic core.

3.5. Experiments on Short-Circuit Behavior

Experiments on short-circuit behavior were based on [28], which specifies test conditions and methods as well as the evaluation of transformer behavior.

Transformer terminal fault situations are multiple, e.g., phase-to-ground short-circuit, short-circuit between two or all phases with or without grounding, etc.

The most critical situation for the transformer is when a three-phase short-circuit occurs between the secondary terminals, and under these conditions, tests are carried out consisting of nine short-circuit tests on each of the two LV windings distributed on each extreme and nominal plot (1, 3, and 5).

For three-phase transformers, the r.m.s. value of the symmetrical short-circuit current I was calculated as follows:

$$I = \frac{U}{\sqrt{3}(Z_t + Z_S)} \text{ [kA]}, \quad (1)$$

where Z_S is the short-circuit impedance of the system (Ω).

$$z_s = \frac{U_S^2}{S} \text{ [}\Omega\text{/phase]} \text{ (equivalent star connection)} \quad (2)$$

where:

U_S is the maximum voltage of the system (kV);

S is the short-circuit apparent power of the system (MVA);

U is rated voltage at tap 1, 3, or 5 in kV;

Z_t is the transformer short-circuit impedance (Ω /phase) calculated as follows:

$$z_t = \frac{Z_t \times U_r^2}{100 \times S_r} \text{ [}\Omega\text{/phase]} \quad (3)$$

where:

Z_t is the percentage of the measured short-circuit impedance at the rated current and the frequency at the main tap and at the reference temperature;

S_r is the rated power of the transformer (MVA);

For taps other than the main tap:

U is the tap voltage of the winding in question (kV);

Z_t is the short-circuit impedance of the transformer with respect to the winding and taps in question (kV).

For autotransformers and transformers with more than two windings, the overcurrents in the windings are determined based on the transformer and system impedance values. The different types of faults that can occur in the system during operation must be taken into account [29].

The characteristics of each system must be specified (at least the short-circuit apparent power level and the transformation ratio between the zero-sequence impedance and the positive-sequence impedance). Following the system analysis (Figure 1) performed on the 8400 kVA power transformer with two identical LV windings used in the tests, the transformer was treated as two transformers with a common 2×4200 kVA HV winding, and measurements were taken separately on each LV winding with a common HV winding.

The transformer short-circuit current rating is based on the maximum short-circuit current under all operating conditions and takes into account transformer voltage regulation. The purpose of the short-circuit impedance requirements is to limit the short-circuit current values to what the system, the inverter, and the transformer can tolerate.

Possible short-circuit situations in the DPV generation system:

- Short-circuit on the high-voltage side of the transformer inverter, between the transformer and the grid [1], as shown in Figure 4a. In this case, the source of the main short-circuit current is from the power system. During the short-circuit, the inverter current is controlled by semiconductors and does not depend on the transformer impedance; initially, the peak and symmetrical short-circuit currents are the same as (or up to 150% higher than) the rated short-circuit current of the inverter;
- Short-circuit on the low voltage side of the transformer inverter, between the transformer and the inverter, as shown in Figure 4b.

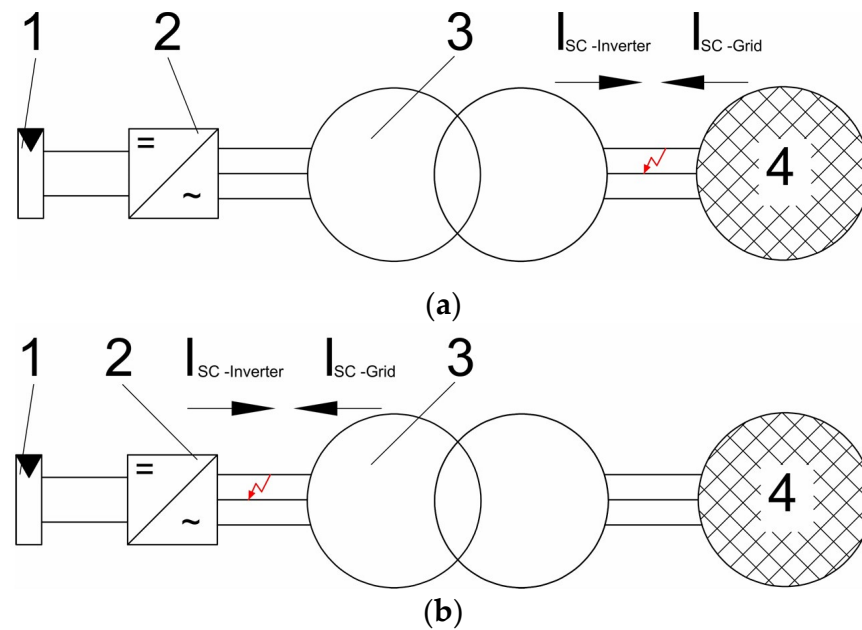


Figure 4. Example of a short-circuit:(a) on the power grid side of the transformer and (b) on the low-voltage side of the transformer, where: 1—PV panels; 2—inverter; 3—transformer; 4—grid.

The main short-circuit current comes from the grid and is limited by the transformer impedance. The short-circuit current of the inverter is equal to the rated current of the inverter.

For the three-winding transformer used in the tests, the fault can occur in either the primary or secondary winding. Considering this, the transformer was analyzed as two transformers with common high-voltage winding 2×4200 kVA.

For multi-winding transformers, it is recommended to analyze the short-circuit currents from each low-voltage input to each high-voltage output and from the input windings to the output winding [1].

The short-circuit currents from the input of one winding to the input of another winding are also analyzed. Faults may occur on one or both input windings and on the output of the high-voltage winding. The winding layout of a multi-winding transformer affects the magnitude and distribution of short-circuit forces. These forces, which affect the mechanical integrity of the winding layout (Figure 2), are an important design consideration.

Using the measured values in Table 1 and formulas (1–3), the test parameters in Tables 2 and 3 are as follows.

Table 2. Ability to withstand the dynamic effects of a short-circuit on 2U2V2W LV winding.

No. of Short-Circuit Tests.		3	3	3
Tapping	No.	1	3	5
	Voltage (kV)	34.65	33	31.35
	Short-circuit time (s)	0.25	0.25	0.25
	Current peak value (A)	2307.5	2442.8	2583.4
	Current r.m.s. value (A)	934.2	988.9	1045.9
	Value of factor $k\sqrt{2}$	2.47	2.47	2.47
	Experiment scheme type		Three-phase	
	Short-circuit type		Pre-set	

Table 3. Ability to withstand the dynamic effects of a short-circuit on 3U3V3W LV winding.

No. of Short-Circuit Tests.		3	3	3
Tapping	No.	1	3	5
	Voltage (kV)	34.65	33	31.35
	Short-circuit time (s)	0.25	0.25	0.25
	Current peak value (A)	2241.3	2372.2	2498.3
	Current r.m.s. value (A)	911.1	964.3	1019.7
	Value of factor $k\sqrt{2}$	2.46	2.46	2.45
	Experiment scheme type	Three-phase		
	Short-circuit type	Pre-set		

where:

$$i = I \times k \times \sqrt{2} \quad (4)$$

i is the amplitude of the first peak of the short-circuit current;

$k \times \sqrt{2}$ is the peak factor as per [28].

The scheme used for the experiments is shown in Figure 5.

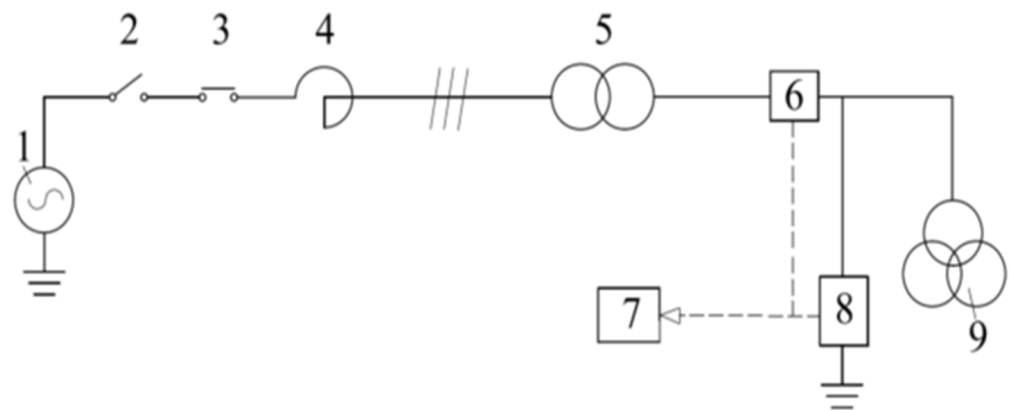


Figure 5. High-power circuit for power testing, where: 1—power generator; 2—master maker; 3—master breaker; 4—power reactor; 5—step-up transformers; 6—current measurement; 7—measurement system; 8—voltage measurement device; 9—tested object.

Under these conditions, by applying nominal voltages to the HV winding 1UVW and three-phase short-circuiting to the LV winding 2UVW, nine tests were carried out, three each on plots 1, 3, and 5, resulting in nine oscillograms with the following average current values, as follows.

The values obtained in this experiment on tap 1 with short-circuit terminals 2U2V2W (Figure 6): voltage between phases, $U_{1U1V} = 29.9$ kV; $U_{1V1W} = 29.9$ kV; $U_{1W1U} = 30.6$ kV; short-circuit current peak value on $I_{1U} = 2329$ A; effective equivalent current $I_{1U} = 878$ A; $I_{1V} = 894$ A; $I_{1W} = 882$ A; test duration $t = 250$ ms.

The values obtained in this experiment on tap 3 with short-circuit terminals 2U2V2W (Figure 7): voltage between phases, $U_{1U1V} = 27.5$ kV; $U_{1V1W} = 27.9$ kV; $U_{1W1U} = 27.6$ kV; short-circuit current peak value on $I_{1V} = 2522$ A; effective equivalent current $I_{1U} = 929$ A; $I_{1V} = 951$ A; $I_{1W} = 886$ A; test duration $t = 250$ ms.

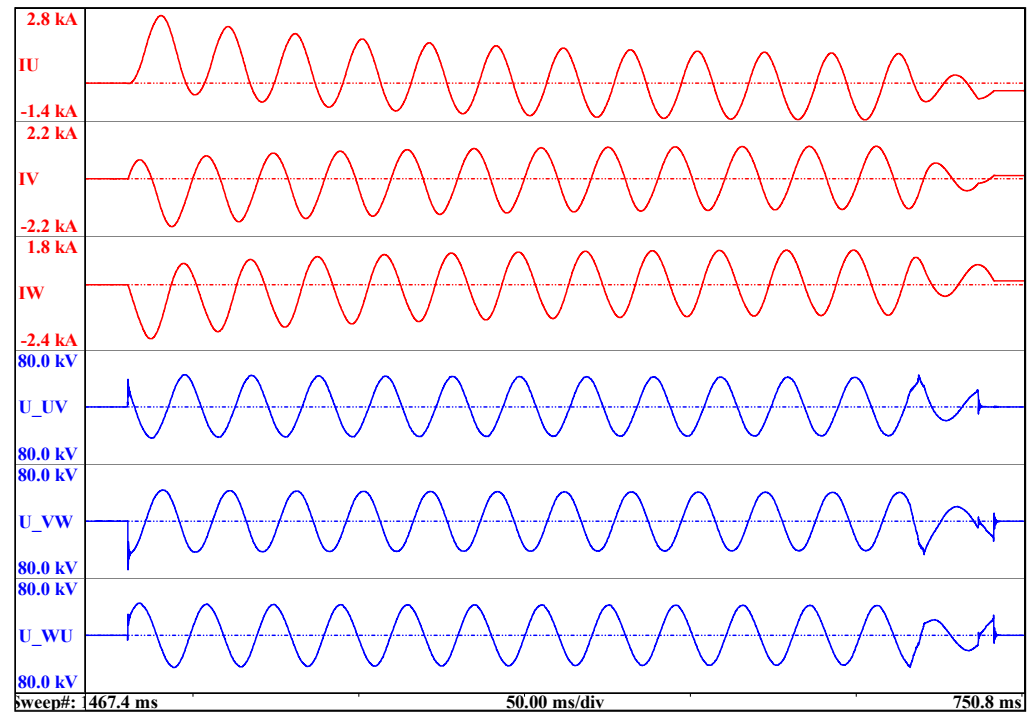


Figure 6. Oscillograms recorded in the second experiment on tap 1 with short-circuit terminals 2U2V2W.

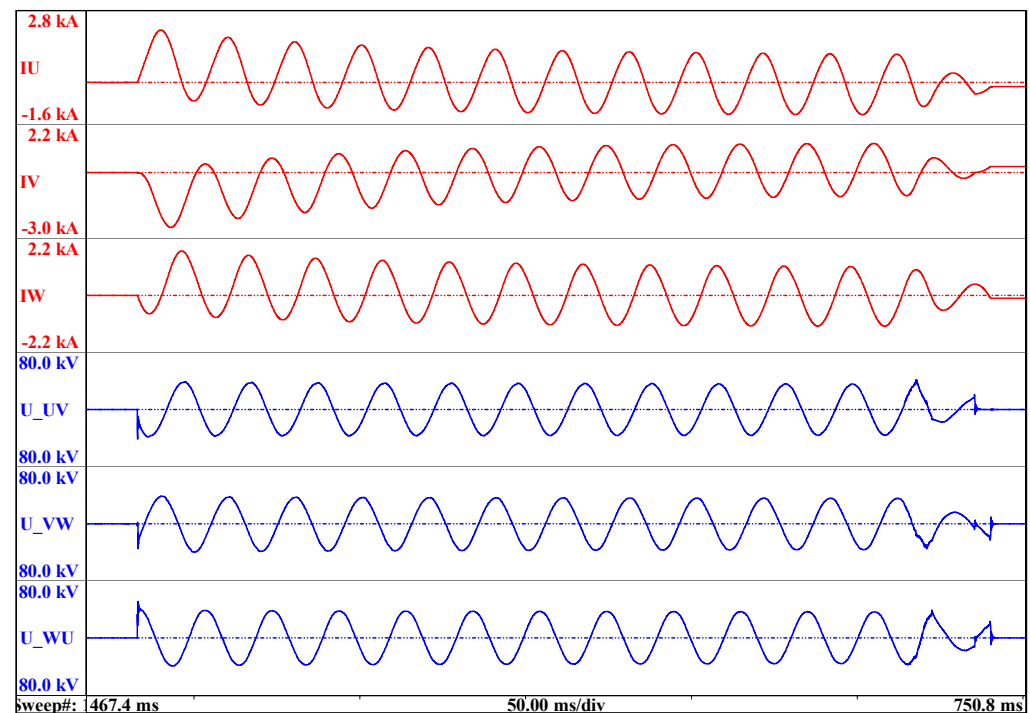


Figure 7. Oscillograms recorded in the second experiment on tap 3 with short-circuit terminals 2U2V2W.

The values obtained in this experiment on tap 5 with short-circuit terminals 2U2V2W (Figure 8): voltage between phases, $U_{1U1V} = 26.6$ kV; $U_{1V1W} = 25.5$ kV; $U_{1W1U} = 26.8$ kV; short-circuit current peak value on $I_{1W} = 2580$ A; effective equivalent current $I_{1U} = 959$ A; $I_{1V} = 1042$ A; $I_{1W} = 1017$ A; test duration $t = 250$ ms.

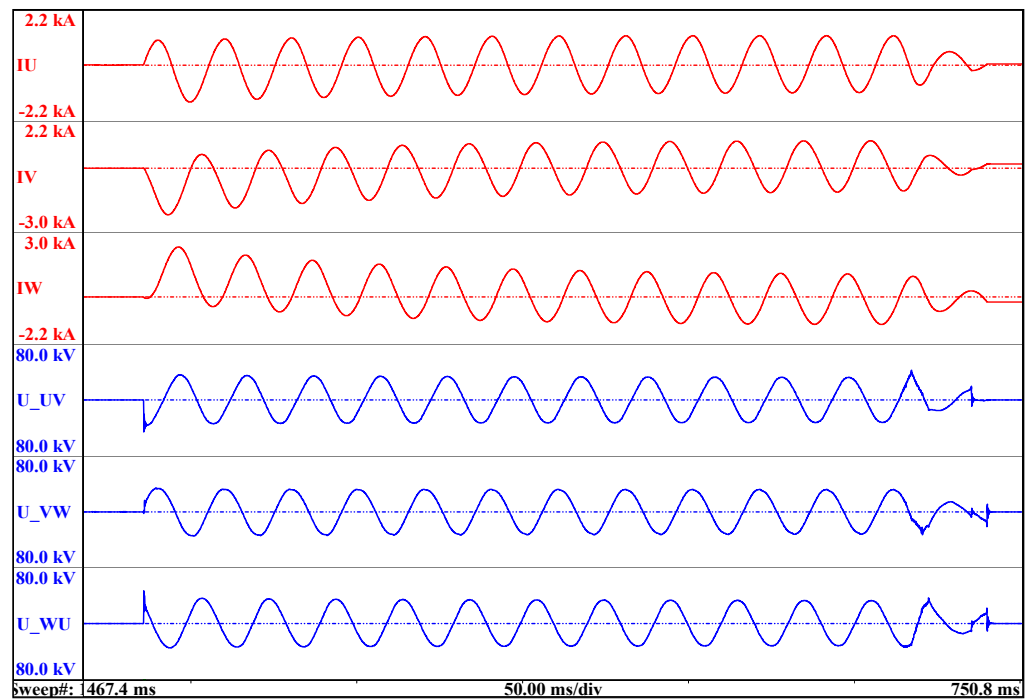


Figure 8. Oscillograms recorded in the second experiment on tap 5 with short-circuit terminals 2U2V2W.

During these experiments, the 3UVW winding was in a no-load condition.

Nine other tests were carried out under similar conditions by applying a nominal voltage to the HV winding and short-circuiting the LV winding 3UVW, and the oscillograms considered significant are shown below:

The values obtained in this experiment on tap 1 with short-circuit terminals 3U3V3W (Figure 9): voltage between phases, $U_{1U1V} = 27.9$ kV; $U_{1V1W} = 27$ kV; $U_{1W1U} = 28.3$ kV; short-circuit current peak value on $I_{1W} = 2336$ A; effective equivalent current $I_{1U} = 827$ A; $I_{1V} = 848$ A; $I_{1W} = 887$ A; test duration $t = 250$ ms.

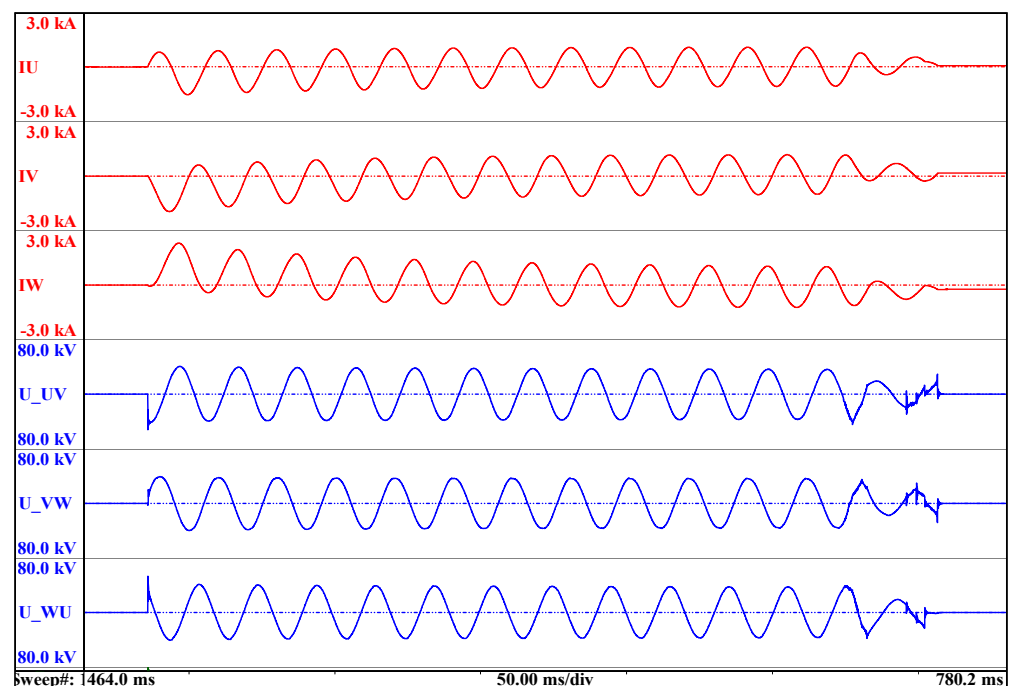


Figure 9. Oscillograms recorded in the third experiment on tap 1 with short-circuit terminals 3U3V3W.

The values obtained in this experiment on tap 3 with short-circuit terminals 3U3V3W (Figure 10): voltage between phases, $U_{1U1V} = 25.6$ kV; $U_{1V1W} = 26.3$ kV; $U_{1W1U} = 26.6$ kV; short-circuit current peak value on $I_{1V} = 2482$ A; effective equivalent current $I_{1U} = 910$ A; $I_{1V} = 945$ A; $I_{1W} = 886$ A; test duration $t = 250$ ms.

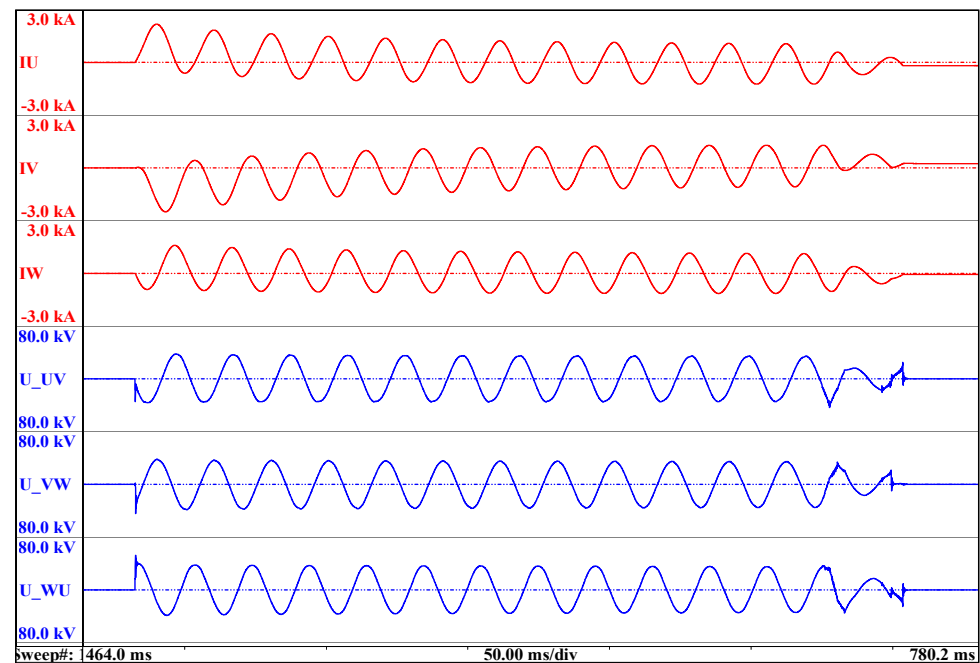


Figure 10. Oscillograms recorded in the third experiment on tap 3 with short-circuit terminals 3U3V3W.

The values obtained in this experiment on plot 5 with short-circuit terminals 3U3V3W (Figure 11): voltage between phases, $U_{1U1V} = 24.6$ kV; $U_{1V1W} = 24.7$ kV; $U_{1W1U} = 25.2$ kV; short-circuit current peak value on $I_{1U} = 2617$ A; effective equivalent current $I_{1U} = 980$ A; $I_{1V} = 924$ A; $I_{1W} = 937$ A; test duration $t = 250$ ms.

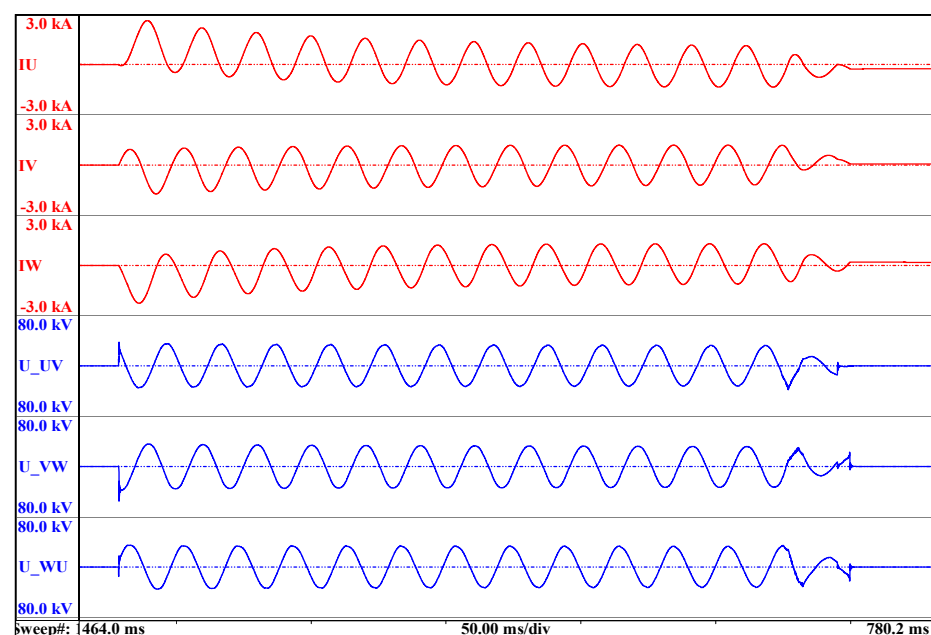


Figure 11. Oscillograms recorded in the third experiment on tap 5 with short-circuit terminals 3U3V3W.

During these experiments, the 2UVW winding was in a no-load condition.

After each short-circuit test, the short-circuit reactance was measured and, according to Tables 4 and 5, the values obtained differ from those measured before the tests by less than 7.5%, which is the maximum permissible limit for the transformer to pass the test.

Table 4. Inductance values on 2U2V2W LV winding.

Tapping	Inductances (mH)			Inductances Variation (%)			
	UV	VW	WU	UV (%)	VW (%)	WU (%)	
1	123.29	124.47	125.15	Before	5.63	6.43	6.00
	130.24	132.48	132.66	After			
3	110.18	111.23	111.88	Before	5.72	6.49	6.05
	116.49	118.45	118.65	After			
5	98.24	99.2	99.79	Before	5.73	6.48	6.12
	103.87	105.63	105.9	After			

Inductance values were measured with an RLC bridge to an accuracy of 0.1%.

Table 5. Inductance values on 3U3V3W LV winding.

Tapping	Inductances (mH)				Inductances Variation (%)		
	UV	VW	UV	VW	UV	VW	UV
1	127.76	128.71	128.76	Before	3.31	3.12	2.67
	132	132.73	132.2	After			
3	114.21	115	115.13	Before	3.36	3.19	2.67
	118.05	118.67	118.21	After			
5	101.87	102.57	102.7	Before	3.42	3.22	2.74
	105.36	105.88	105.52	After			

Inductance values were measured with an RLC bridge to an accuracy of 0.1%.

Routine tests were also repeated and the results are shown in Table 6, showing no differences above the acceptable limits.

The measurement of the short-circuit reactance is a fundamental criterion for evaluating the short-circuit behavior of a transformer, highlighting the smallest winding displacements according to [28].

Depending on the design of the transformer, the permissible reactance variation before and after a short-circuit can be 4 or 7.5%. The permissible variation means that the transformer continues to operate after the short-circuit because it has not been subjected to any major faults.

In the studied transformer, it can be seen that the low voltage winding 2UVW, which is closest to the core, has a lower short-circuit reactance, and therefore higher short-circuit currents and displacement of the LV winding, and the reactance variation is 6.5%, while in the winding 3UVW, further from the core, with higher short-circuit reactance and lower currents, the reactance variation does not exceed 3.5%.

Table 6. Values obtained from measurements of winding resistance, voltage ratio, wiring diagram and vector group, no-load, and short-circuit losses after the short-circuit tests.

Measurement of Winding Resistance Temperature 25.3 (°C)	Tape	1U1V (mΩ)	1V1W (mΩ)	1U1W (mΩ)								
HV winding	1	434.09	433.98	433.55								
	2	423.79	423.67	423.21								
	3	413.09	412.94	412.49								
	4	402.67	402.94	402.05								
	5	391.99	391.87	391.39								
LV winding		2U2V (μΩ) 408.75	2V2W (μΩ) 433.47	2W2U (μΩ) 437.02								
		3U3V (μΩ) 449.53	3V3W (μΩ) 455.39	3W3U (μΩ) 468.28								
	Measurement of voltage ratio vector group Dyn11	1U-1V1W/2U-2W			1V-1W1U/2V-2U			1W-1U1V/2W-2V				
		Tape	Calc.	Meas.	Dev.	Tape	Calc.	Meas.	Dev.	Tape	Calc.	Meas.
1		45.466	45.373	-0.21	1	45.466	45.386	-0.18	1	45.466	45.392	-0.16
2		44.384	44.330	-0.12	2	44.384	44.338	-0.10	2	44.384	44.341	-0.10
3		43.301	43.279	-0.05	3	43.301	43.284	-0.04	3	43.301	43.286	-0.04
4	42.219	42.220	0.00	4	42.219	42.228	0.02	4	42.219	42.229	0.02	
5	41.136	41.168	0.08	5	41.136	41.172	0.09	5	41.136	41.174	0.09	
	Tape	Calc.	Meas.	Dev.	Tape	Calc.	Meas.	Dev.	Tape	Calc.	Meas.	Dev.
	1	45.466	45.388	-0.17	1	45.466	45.395	-0.16	1	45.466	45.397	-0.15
	2	44.384	44.335	-0.11	2	44.384	44.341	-0.10	2	44.384	44.342	-0.09
	3	43.301	43.279	-0.05	3	43.301	43.284	-0.04	3	43.301	43.286	-0.04
	4	42.219	42.224	0.01	4	42.219	42.229	0.02	4	42.219	42.229	0.02
	5	41.136	41.166	0.07	5	41.136	41.172	0.09	5	41.136	41.173	0.09
Measurement of short-circuit impedance and load loss TAP POSITION-1	4200 kVA 2U-2V-2W short-circuited				4200 KVA 3U-3V-3W short-circuited							
		Current A	Voltage V	Power W		Current A	Voltage V	Power W				
	U	69.734	1499	8638	U	69.152	1513	10,006				
	V	70.940	1488	9147	V	70.008	1502	9315				
	W	69.143	1494	11,091	W	70.027	1507	11,499				
	Avrg.	70.272	1494	Σ: 28,876	Avrg.	69.729	1507	Σ: 30,820				
	Δcorr.	0.9958	Γcorr.	0.9917	Δcorr.	1.0036	Γcorr.	1.0072				
		$I_n = 69.982 \text{ A}$	$U_n = 2449.12 \text{ V}$	$P_k = 28,638 \text{ W}$		$I_n = 69.982 \text{ A}$	$U_n = 2610.78 \text{ W}$	$P_k = 30,438 \text{ W}$				
		$P_{k(75^\circ\text{C})} = 28,199 \text{ W}$	$U_{k(75^\circ\text{C})} \% = 7.46$			$P_{k(75^\circ\text{C})} = 29,973 \text{ W}$	$U_{k(75^\circ\text{C})} \% = 7.59$					
	Measurement of short-circuit impedance and load loss TAP POSITION-3	4200 kVA 2U-2V-2W short-circuited				4200 kVA 3U-3V-3W short-circuited						
		Current A	Voltage V	Power W		Current A	Voltage V	Power W				
U		72.742	1398.00	8512	U	72.810	1424.00	10,043				
V		73.977	1386.00	9032	V	73.695	1414.00	9387				
W		73.122	1392.00	10,954	W	73.690	1419.00	11,558				
Avrg.		73.280	1392.00	Σ: 28,498	Avrg.	73.398	1419.00	Σ: 30,988				
Δcorr.		1.0027	Γcorr.	1.0054	Δcorr.	1.0011	Γcorr.	1.0022				
		$I_n: 73.481 \text{ A}$	$U_n: 2411.01 \text{ V}$	$P_k: 28,654 \text{ W}$		$I_n = 73.481 \text{ A}$	$U_n = 2457.78 \text{ V}$	$P_k = 31,058 \text{ W}$				
		$P_{k(75^\circ\text{C})} = 28,270 \text{ W}$	$U_{k(75^\circ\text{C})} \% = 7.35$			$P_{k(75^\circ\text{C})} = 30,506 \text{ W}$	$U_{k(75^\circ\text{C})} \% = 7.49$					
Measurement of short-circuit impedance and load loss TAP POSITION-5		4200 kVA 2U-2V-2W short-circuited				4200 KVA 3U-3V-3W short-circuited						
		Current A	Voltage V	Power W		Current A	Voltage V	Power W				
	U	76.693	1314	8594	U	76.891	1324	10,149				
	V	77.960	1302	9094	V	77.798	1332	9501				
	W	77.070	1308	11,040	W	77.807	1336	11,690				
	Avrg.	77.241	1308	Σ: 28,728	Avrg.	77.499	1337	Σ: 31,340				
	Δcorr.	1.0013	Γcorr.	1.0027	Δcorr.	0.9980	Γcorr.	0.9961				
		$I_n: 77.348 \text{ A}$	$U_n: 2265.52 \text{ V}$	$P_k: 28,808 \text{ W}$		$I_n: 77.348 \text{ A}$	$U_n: 2315.17 \text{ V}$	$P_k: 31,219 \text{ W}$				
		$P_{k(75^\circ\text{C})} = 28,461 \text{ W}$	$U_{k(75^\circ\text{C})} \% = 7.26$			$P_{k(75^\circ\text{C})} = 30,703 \text{ W}$	$U_{k(75^\circ\text{C})} \% = 7.40$					

Table 6. Cont.

Measurement of Winding Resistance Temperature 25.3 (°C)	Tape	1U1V (mΩ)			1V1W (mΩ)			1U1W (mΩ)				
Measurement of no-load loss and current	Excitation Factor 90%				Excitation Factor 100%				Excitation Factor 110%			
		Current A	Voltage V	Power W	Current A	Voltage V	Power W	Current A	Voltage V	Power W		
	U	6.468	344.58	2059.0	U	11.676	382.94	3098.0	U	55.518	416.52	9020.0
	V	3.884	342.33	1108.0	V	7.797	379.53	1435.0	V	39.849	422.39	680.0
	W	6.100	341.97	1540.0	W	11.725	380.73	1760.0	W	60.357	418.66	111.2
	Avrg.	5.484	342.96	Σ: 4707	Avrg.	10.399	381.07	Σ: 6293	Avrg.	51.908	419.19	Σ: 9636
	$V_{RMS} = 594.7$ V	$V_{MEAN} = 594.0$ V	$P_0 = 4702$ W	$V_{RMS} = 661.9$ V	$V_{MEAN} = 660.0$ V	$P_{0GUARANTEED} = 7200$ W + 15%	$V_{RMS} = 740.7$ V	$V_{MEAN} = 726.1$ V				
$I_0 = 5.484$ A	$I_0 = 0.15\%$	$I_0 = 10.399$ A	$I_0 = 0.28\%$	$P_0 = 9613$ W	$I_0 = 51.908$ A	$I_0 = 1.41\% P_0 = 9613$ W						

Calc.—calculated; Meas.—measured; Dev.—deviation; Avrg.—average; Δcorr.—current correction; Γcorr.—power correction; Σ—sum power.

3.6. Frequency Response Analysis

Transformer behavior is also confirmed by frequency response analysis (FRA), which is used as a recommendation for transformer fault detection [30].

Frequency response analysis is a method that provides information about several types of faults occurring in the transformer, coil insulation faults, tap changer faults, and coil displacement faults, but for none of the faults does it provide quantitative data to assess the severity of the fault.

Therefore, this method is only a recommendation, not a requirement, for the evaluation of the condition of the transformer after a short-circuit.

In this experiment, a low-voltage signal was applied between one terminal of the test object and the tank. The voltage measured at this input terminal was used as the reference signal, and the second voltage signal (the response signal) was measured at the second terminal with respect to the tank. The amplitude of the frequency response is the ratio of the scalar response signal (V_{out}) to the scalar reference voltage (V_{in}), shown in Figure 12 in dB as a function of frequency. The phase of the frequency response is the phase difference between V_{in} and V_{out} , expressed in degrees.

The frequency response measurement was performed at an impedance of 50 ohms. Any coaxial cable connected between the terminal of the test object and the meter was of appropriate impedance.

In all cases, the transformer was fully equipped as it would be in service. The core and connection to the tank frame were in place and the tank was grounded. The performance of the measuring instrument was verified by measuring the response to a known test object and verifying that the measured amplitude ratio matched the assumed response over the entire frequency range.

Figure 12 shows the comparative frequency response before and after the short. The representation of the frequency response between 10 Hz and 1 MHz is in logarithmic scale to make it easier to highlight defects and locate them on the active part (core, windings, terminals).

The frequency range between 1 kHz and 1 MHz corresponding to the windings shows an identical variation before and after the test, which means that there is no change in the winding on UVW phases at high and low voltage, which is also confirmed by the variation in the short-circuit reactance.

Due to the fact that the frequency response of the transformer is fundamentally related to the structure of the core and windings, various frequency response characteristics have been obtained. In Figure 12, the frequency response can be divided into three regions: the low-frequency region created by the core, the mid-frequency region created by the

winding interaction, and the high-frequency region controlled by the individual winding structure and internal connections. In Figure 12, the region up to 2 kHz is the core influence region and the response is dominated by the core magnetizing inductances and the bulk capacitances of the transformer. The middle phase has a single anti-resonance in this frequency region due to the symmetric magnetic reluctance paths observed by the middle phase of the core through the other two phases. The outer phases generally have two anti-resonances since they experience two different magnetic reluctance paths, one through the nearest phase and one through the furthest phase. The residual magnetization of the core also influences the frequency response in this region.

The response in the intermediate frequency region (between 2 kHz and 20 kHz) is mostly affected by the coupling between the windings, which depends significantly on the arrangement and connections of the windings and shows a very strong coupling in Figure 12.

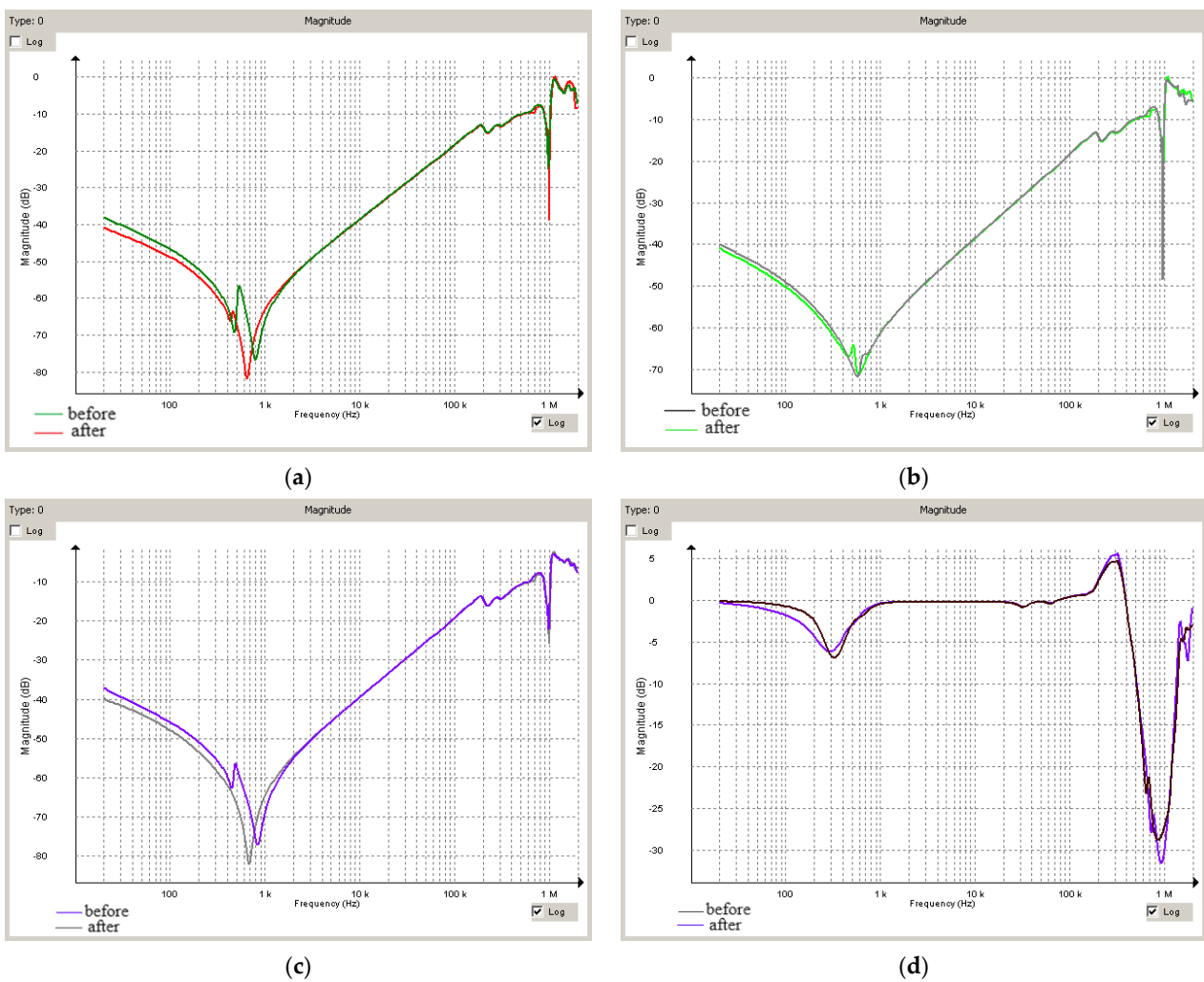
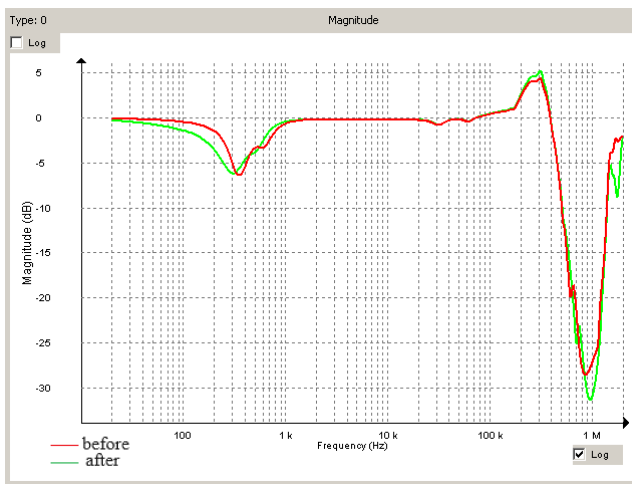
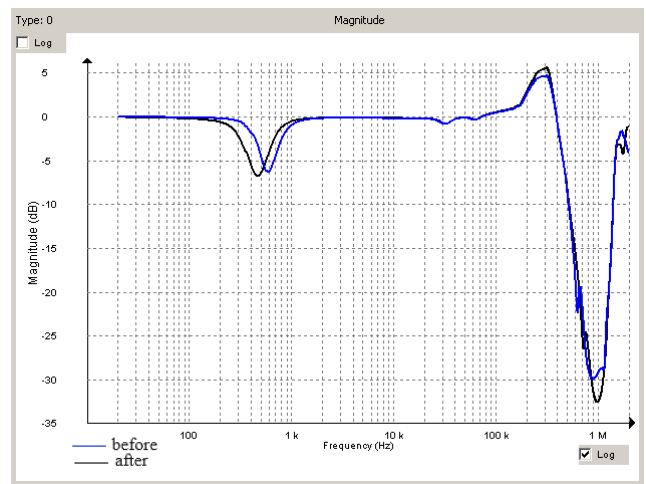


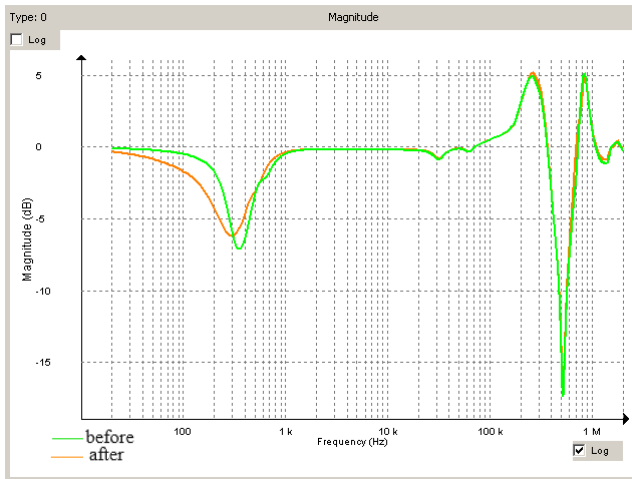
Figure 12. Cont.



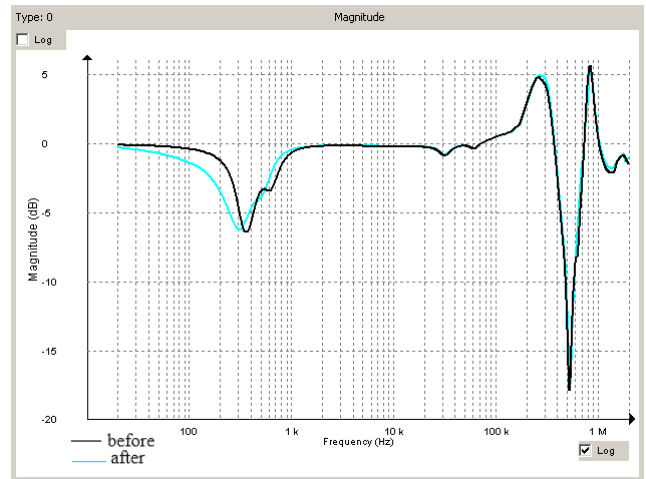
(e)



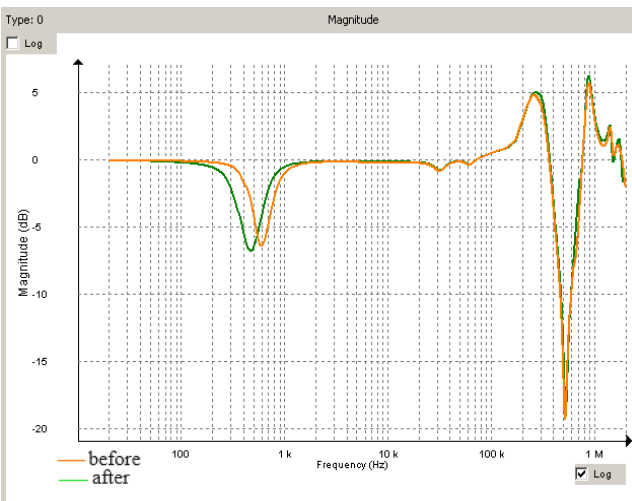
(f)



(g)



(h)



(i)

Figure 12. Frequency response analysis before and after on (a) 1u-1v; (b) 1v-1w; (c) 1w-1u; (d) 2u-2c; (e) 2v-2w; (f) 2w-2u; (g) 3u-3v; (h) 3v-3w; (i) 3w-3u.

In the winding structure influence (high frequency) region (between 20 kHz and 1 MHz in our case), the response is determined by the winding leakage inductances together with the winding series and ground capacitances. In this region, the series capacitance is the most influential factor in determining the shape of the response. In Figure 12, the response of the HV winding shows a decreasing amplitude trend with few resonances and anti-resonances. The highest frequencies above 1 MHz will not be discussed because the response is less repeatable and is influenced by the measurement setup.

4. Conclusions

All experiments presented in this paper were performed on an 8.4 MVA transformer with one 33 kV HV winding and two 0.66 kV LV windings with the following characteristics: transformer rated power, $S_N = 8400$ kVA; HV side voltage, $U_{HV} = 33$ kV $\pm 2 \times 2.5\%$; LV side voltage, $U_{LV} = 0.66$ kV – 0.66 kV; rated current of energized winding, $I_N = 147$ A/3674 – 3674 A; vector group, $\Delta Y11Y11$; cooling type, Oil Natural Air Natural (ONAN); windings, aluminum conductor, non-circular (oval).

The significant development of photovoltaic energy sources has led to the emergence of a new generation of distribution transformers designed to withstand the specific stresses of operation with inverters on the low-voltage side.

The main conclusions from the experiments are as follows:

- No-load transformer operation requires low iron losses (PFe);
- Experiments confirm that the arrangement of the windings (split or alternated) leads to accepted short-circuit behavior and proves that unbalanced and asymmetrical regimes require special attention in design;
- Surges during thyristor switching (max 500 V/ μ s) require the shielding of LV windings and additional insulation;
- Low-voltage windings with two, three, or more identical windings present terminal connection problems;
- The separation of the LV and HV windings by columns is necessary to eliminate the disadvantages caused by unbalanced and unsymmetrical conditions;
- Attempting to demonstrate compliance with international standards is a difficult challenge;

After the experiments, it was found that:

- The results of the short-circuit tests and the measurements and checks performed during the tests do not reveal any condition of faults;
- The dielectric tests and other routine tests, when applicable, were successfully repeated, and the lightning impulse test, if specified, was successfully performed;
- The out-of-tank inspection does not reveal any defects such as displacements, shifts of laminations, or deformations of windings, connections, or supporting structures so significant that they might endanger the safe operation of the transformer;
- The frequency response analysis (FRA) is sufficient to detect changes in the active part;
- No traces of internal electrical discharge were found;
- The short-circuit reactance values, in ohms, evaluated for each phase at the end of the tests, do not differ from the original values by more than 7.5% for transformers with non-circular concentric coils with a short-circuit impedance of 3% or more. The value of 7.5% may be reduced by agreement between the manufacturer and the purchaser but not below 4%;
- The guaranteed uncertainty for the measured voltages and currents, taking into account the total measuring system, is less than 3%, unless mentioned otherwise.

Future work will analyze the thermal design and the load curve of this type of transformer correlated with specific ambient conditions at the installation site. It is very important to note the increased loads when operating with an additional reactive power supply.

Author Contributions: Conceptualization, C.-E.S., C.D. and D.O.; methodology, C.-E.S., C.D. and D.O.; software, C.-E.S. and M.N.; validation, C.-E.S., C.D., D.O. and M.N.; formal analysis, C.-E.S., C.D., D.O., M.N., D.I. and M.-C.N.; investigation, C.-E.S., D.I. and M.-C.N.; resources, C.-E.S.; data curation, C.-E.S., C.D., D.O., M.N., D.I. and M.-C.N.; writing—original draft preparation, C.-E.S.; writing—review and editing, C.-E.S., M.N. and D.I.; visualization, C.-E.S., C.D., D.O., M.N., D.I. and M.-C.N.; supervision, C.-E.S., C.D., D.O., M.N., D.I. and M.-C.N.; project administration, C.-E.S.; funding acquisition, C.-E.S. All authors have read and agreed to the published version of the manuscript.

Funding: This research was funded by the Ministry of Research, Innovation and Digitization of Romania as part of the NUCLEU Program: PN 23 33 02 01.

Data Availability Statement: Not applicable.

Conflicts of Interest: The authors declare no conflict of interest.

References

1. *IEEE C.57.159*; IEEE Guide for Transformers for Application in Distributed Photovoltaic (DPV) Power Generation Systems. IEEE Power and Energy Society: New York, NY, USA, 2016.
2. *IEEE C.57.110*; IEEE Recommended Practice for Establishing Transformer Capability When Supplying Non-Sinusoidal Load Currents. IEEE Power and Energy Society: New York, NY, USA, 1998.
3. *IEEE std 519*; IEEE Recommended Practices and Requirements for Harmonic Control in Electrical Power Systems. IEEE Power and Energy Society: New York, NY, USA, 1992.
4. Pezeshki, H.; Wolfs, P.J.; Ledwich, G. Impact of High PV Penetration on Distribution Transformer Insulation Life. *IEEE Trans. Power Deliv.* **2014**, *29*, 1212–1220. [[CrossRef](#)]
5. *IEC 60076-1*; Power Transformers—Part 1: General. IEEE Power and Energy Society: New York, NY, USA, 2011.
6. *IEC 60076-11*; Power Transformers—Part 11: Dry-Type. IEEE Power and Energy Society: New York, NY, USA, 2004.
7. *IEC 60076-14*; Power Transformers—Part 14: Liquid-Immersed Power Transformers Using High-Temperature Insulation Materials. IEEE Power and Energy Society: New York, NY, USA, 2013.
8. *IEC 60076-16*; Power Transformers—Part 16: Transformers for Wind turbine Applications. IEEE Power and Energy Society: New York, NY, USA, 2011.
9. *IEC 60076-7*; Power Transformers—Part 7: Loading Guide for Mineral-Oil-Immersed Power Transformers. IEEE Power and Energy Society: New York, NY, USA, 2005.
10. Krishnan, R.; Nair, K.R.M. Transformer for Distributed Photovoltaic (DPV) Generation. In Proceedings of the International Conference on Electrical, Electronics, Communication, Computer, and Optimization Techniques (ICEECCOT), Mysuru, India, 14–15 December 2018; pp. 1659–1663. [[CrossRef](#)]
11. Wu, Y.; Liu, L.; Shi, C.; Ma, K.; Li, Y.; Mu, H. Research on Measurement Technology of Transformer No-load Loss Based on Internet of Things. In Proceedings of the IEEE 8th International Conference on Advanced Power System Automation and Protection (APAP), Xi'an, China, 21–24 October 2019; pp. 150–153. [[CrossRef](#)]
12. Salceanu, C.-E.; Nicola, M.; Nicola, C.; Ocoleanu, D.C.; Dobrea, C.; Iovan, D.; Enache, S. Numerical Simulations and Experimental Tests for the Analysis of Capacitive Load Switching in Power Circuits. In Proceedings of the International Conference and Exposition on Electrical and Power Engineering (EPE), Iasi, Romania, 20–22 October 2022; pp. 409–414. [[CrossRef](#)]
13. Sălceanu, C.-E.; Nicola, M.; Nicola, C.-I.; Ocoleanu, D.; Dobrea, C.; Iovan, D.; Enache, S. Experimental Study on the Behavior of Aluminum Fuse Element Inside 24 kV, 50 kA High-Voltage Fuses. *Energies* **2022**, *15*, 7171. [[CrossRef](#)]
14. Salceanu, C.-E.; Nicola, M.; Ocoleanu, D.; Iovan, D.; Enache, S. Experimental Study of HBC Fuses with Aluminium Fuse Element at Minimum Rated Breaking Current. In Proceedings of the International Conference on Applied and Theoretical Electricity (ICATE), Craiova, Romania, 27–29 May 2021; pp. 1–6. [[CrossRef](#)]
15. Huang, Z.; Wang, R.; Rapp, K.J.; Liu, G. Test Comparison Study on a Natural Ester Retro-filled 220kV Power Transformer. In Proceedings of the IEEE International Conference on High Voltage Engineering and Application (ICHVE), Beijing, China, 6–10 September 2020; pp. 1–4. [[CrossRef](#)]
16. Schweiger, E.; Ettl, C.; Hennig, E.G.; Riegler, S.; Stoessl, M.; Bose, S. Resilience solutions for bypassing power transformers and recommendations of site commissioning tests. In Proceedings of the IEEE Power & Energy Society General Meeting (PESGM), Atlanta, GA, USA, 4–8 August 2019; pp. 1–5. [[CrossRef](#)]
17. Takacs, K.; Frivaldsky, M. Simulation design of residential smart-grid based on solid-state transformer. In Proceedings of the 2022 ELEKTRO (ELEKTRO), Krakow, Poland, 23–26 May 2022; pp. 1–6. [[CrossRef](#)]
18. Yue, S.; Ji, W.; Xu, J.; Zhang, J.; Wang, S. Research on Black Start of High-Proportion Renewable Energy System Based on Solar-Storage Generation System. In Proceedings of the IEEE Sustainable Power and Energy Conference (iSPEC), Perth, Australia, 4–7 December 2022; pp. 1–6. [[CrossRef](#)]
19. De-Paz-Centeno, I.; García-Ordás, M.T.; García-Olalla, Ó.; Girón-Casares, C.; Alaiz-Moretón, H. A Granularity Invariant Method for the Classification of Energy Production Time Series in Photovoltaic Plants. *IEEE Access* **2023**, *11*, 16923–16933. [[CrossRef](#)]

20. Shah, A.M.; Bhalja, B.R.; Patel, R.M.; Bhalja, H.; Agarwal, P.; Makwana, Y.M.; Malik, O.P. Quartile Based Differential Protection of Power Transformer. *IEEE Trans. Power Deliv.* **2020**, *35*, 2447–2458. [[CrossRef](#)]
21. Moscoso, M.; Lloyd, G.J.; Liu, K.; Wang, Z. Improvements to transformer differential protection-Design and test experience. In Proceedings of the 47th International Universities Power Engineering Conference (UPEC), London, UK, 4 September 2012; pp. 1–6.
22. Pires, V.F.; Cabral, A.; Guerreiro, M. Transformer differential protection based on the 3D current trajectory mass center. In Proceedings of the 4th International Conference on Power Engineering, Energy and Electrical Drives, Istanbul, Turkey, 13–17 May 2013; pp. 52–57.
23. Saleh, S.A.; Ozkop, E. ANSI 87T-Based Differential Protection of 3 ϕ Solid-State Transformers. In Proceedings of the IEEE Industry Applications Society Annual Meeting, Detroit, MI, USA, 10–16 October 2020; pp. 1–9. [[CrossRef](#)]
24. Saleh, S.A.M.; Richard, C.; Onge, X.F.S.; McDonald, K.M.; Ozkop, E.; Chang, L.; Alsayid, B. Solid-State Transformers for Distribution Systems—Part I: Technology and Construction. *IEEE Trans. Ind. Appl.* **2019**, *55*, 4524–4535. [[CrossRef](#)]
25. Saleh, S.A.; Ozkop, E.; Alsayid, B.; Richard, C.; Onge, X.F.S.; McDonald, K.M.; Chang, L. Solid-State Transformers for Distribution Systems—Part II: Deployment Challenges. *IEEE Trans. Ind. Appl.* **2019**, *55*, 5708–5716. [[CrossRef](#)]
26. Topolski, Ł. Mitigation of Voltage Swells and Unbalance Caused by Photovoltaic Installations Using a Balancing Transformer and an Automatic Voltage Regulator in Low-Voltage Networks. In Proceedings of the 12th International Conference and Exhibition on Electrical Power Quality and Utilisation (EPQU), Cracow, Poland, 14–15 September 2020; pp. 1–5. [[CrossRef](#)]
27. Pacheco, P.; Cuesto, M.; Burgos, M. Sizing Step-up Transformers for Solar Generation based on Load Profiles Predictability. In Proceedings of the 6th International Advanced Research Workshop on Transformers (ARWtr), Cordoba, Spain, 7–9 October 2019; pp. 37–41. [[CrossRef](#)]
28. IEC 60076-5; Power Transformers—Part 5: Ability to Withstand Short Circuit. IEEE Power and Energy Society: New York, NY, USA, 2006.
29. IEC 60076-8; Power Transformers—Part 8: Application Guide. IEEE Power and Energy Society: New York, NY, USA, 1997.
30. IEC 60076-18; Power Transformers—Part 18: Measurement of Frequency Response. IEEE Power and Energy Society: New York, NY, USA, 2012.
31. She, X.; Huang, A.Q.; Burgos, R. Review of Solid-State Transformer Technologies and Their Application in Power Distribution Systems. *IEEE J. Emerg. Sel. Top. Power Electron.* **2013**, *1*, 186–198. [[CrossRef](#)]
32. Chen, H.; Prasai, A.; Moghe, R.; Chintakrinda, K.; Divan, D. A 50-kVA Three-Phase Solid-State Transformer Based on the Minimal Topology: Dyna-C. *IEEE Trans. Power Electron.* **2016**, *31*, 8126–8137. [[CrossRef](#)]
33. Guillod, T.; Krismer, F.; Kolar, J.W. Protection of MV Converters in the Grid: The Case of MV/LV Solid-State Transformers. *IEEE J. Emerg. Sel. Top. Power Electron.* **2017**, *5*, 393–408. [[CrossRef](#)]
34. Mohan, N.; Undeland, R.M.; Robbins, W.P. *Power Electronics, Converters, Applications and Design*, 2nd ed.; John Wiley & Sons: Hoboken, NJ, USA, 1995; p. 24.
35. Surirey, Q.; Hernandez-Vidal, R.; Renaudineau, H.; Kouro, S.; Cabon, B. Sub-module photovoltaic microinverter with cascaded push-pull and unfolding H-bridge inverter. In Proceedings of the IEEE Southern Power Electronics Conference (SPEC), Puerto Varas, Chile, 4–7 December 2017; pp. 1–6. [[CrossRef](#)]

Disclaimer/Publisher’s Note: The statements, opinions and data contained in all publications are solely those of the individual author(s) and contributor(s) and not of MDPI and/or the editor(s). MDPI and/or the editor(s) disclaim responsibility for any injury to people or property resulting from any ideas, methods, instructions or products referred to in the content.